

# Frequency division multiplexing for interferometric planar Doppler velocimetry

Thomas O. H. Charrett, Ian A. Bledowski, Stephen W. James, and Ralph P. Tatam\*

Engineering Photonics, School of Engineering, Cranfield University, Cranfield, Bedfordshire, MK43 0AL, UK

\*Corresponding author: r.p.tatam@cranfield.ac.uk

Received 19 December 2013; revised 14 May 2014; accepted 29 May 2014;  
posted 30 May 2014 (Doc. ID 203456); published 2 July 2014

A new method of acquiring simultaneously the signal and reference channels used for interferometric planar Doppler velocimetry is proposed and demonstrated. The technique uses frequency division multiplexing (FDM) to facilitate the capture of the requisite images on a single camera, and is suitable for time-averaged flow measurements. Furthermore, the approach has the potential to be expanded to allow the multiplexing of additional measurement channels for multicomponent velocity measurement. The use of FDM for interferometric referencing is demonstrated experimentally with measurements of a single velocity component of a seeded axisymmetric air jet. The expansion of the technique to include multiple velocity components was then investigated theoretically and experimentally to account for bandwidth, crosstalk, and dynamic range limitations. The technique offers reduced camera noise, automatic background light suppression, and crosstalk levels of typically <10%. Furthermore, as this crosstalk is dependent upon the channel modulations applied, it can be corrected for in postprocessing. © 2014 Optical Society of America

OCIS codes: (120.0120) Instrumentation, measurement, and metrology; (120.7250) Velocimetry; (120.3180) Interferometry.

<http://dx.doi.org/10.1364/AO.53.004363>

## 1. Introduction

Measurement of fluid flows is of fundamental importance in engineering for improving design and reducing emissions and noise in a variety of applications, including external aerodynamics, e.g., wind tunnel measurements, and in internal flows such as in turbo machinery. Point optical techniques, such as laser Doppler velocimetry (LDV) [1] use the Doppler frequency shift,  $\Delta\nu$ , of light scattered from particles entrained in a flow to measure the velocity without disturbing the flow. The Doppler shift is related to velocity by

$$\Delta\nu = \frac{\nu_0(\mathbf{o} - \mathbf{i}) \cdot \mathbf{V}}{c}, \quad (1)$$

where  $\nu_0$  is the illumination light frequency,  $\mathbf{V}$  is the velocity of the scattering particles,  $c$  is the free space speed of light, and  $\mathbf{o}$  and  $\mathbf{i}$  are unit vectors in the observation and illumination directions, respectively. The vector  $(\mathbf{o} - \mathbf{i})$  is referred to as the sensitivity vector,  $\hat{\mathbf{s}}$ , and defines the component of velocity measured.

While LDV is a well established and commercially available technique, the undertaking of measurements over an extended area requires a large number of individual highly localized measurements, which can be time consuming and costly. There is, therefore, great interest in techniques that can provide measurements quickly and over large areas. Planar Doppler velocimetry (PDV) [2,3], also known as Doppler global velocimetry (DGV) [4,5], is one such technique that allows the measurement of the distribution of Doppler shifts over a plane defined by a laser light sheet. In conventional PDV [2], a molecular filter is used as a frequency-to-intensity transducer, with a

Doppler shift causing either an increase or decrease in the light transmitted through the filter and recorded by the camera. However, the use of molecular gas filters has several disadvantages; the choice of lasers is limited by the requirements for high-power, single-frequency operation and the ability to tune the emission wavelength to an appropriate absorption line. Second, the molecular filter's transfer function, which determines the velocity range and resolution that can be measured by a PDV system, is determined by the form of the gaseous absorption line, and therefore the sensitivity cannot be varied greatly. Limited changes to the shape of the spectral feature can be made by varying the molecular concentration or the cell temperature, or by the addition of buffer gases to broaden the absorption line [6]. This, however, cannot alter significantly the measurement range. In addition, both the temperature and pressure of the gas cell used in a PDV experiment must be well defined and well controlled to ensure that the absorption line shape is stable, thus limiting systematic errors [7].

Interferometric planar Doppler velocimetry (I-PDV) describes a group of techniques (Doppler picture velocimetry [8–10], Mach–Zehnder interferometric PDV [11,12], and near-resonant interferometry [13,14]) that use optical interferometry to make planar velocity measurements and attempt to overcome some of the limitations of molecular-filter-based PDV. In I-PDV, the molecular filter is replaced with a path-length imbalanced interferometer, and the Doppler-shifted light causes a change in the light intensity distribution in the recorded interference pattern. The magnitude of this change is proportional to the flow velocity and the path-length imbalance in the interferometer. I-PDV has been used for both flow visualization [8] and quantitative velocity measurements [11–15] by evaluating the interferometric phase change that occurs when the light is Doppler frequency shifted. The relationship between the Doppler frequency shift,  $\Delta\nu$ , the optical path length imbalance,  $\Delta l$ , and the change in the phase difference  $\Delta\phi$  is given by

$$\Delta\phi = \frac{2\pi\Delta l}{c} \Delta\nu. \quad (2)$$

Although the laser used in I-PDV systems should still provide a high-power and single optical frequency output, it does not need to be tuned to a specific absorption line. This greatly increases the available choice of laser source and operating wavelength. Another significant advantage of I-PDV systems is that the filter transfer function can be adjusted by changing the path length imbalance of the interferometer, allowing the measurement range and resolution to be adjusted widely. The measurement range for an I-PDV system is determined by the free spectral range, FSR, of the interferometer and can be adjusted by varying the path length imbalance,  $\Delta l$ :

$$\text{FSR} = \frac{c}{\Delta l}. \quad (3)$$

The velocity measurement in an I-PDV system is made by evaluating the interferometric phase, which can be achieved using a single camera. However, it is still necessary to evaluate the phase under two flow conditions, termed the signal phase and the reference phase (the latter under zero-velocity-flow conditions). If the images necessary to evaluate the reference and signal phases are captured sequentially, then errors can be introduced due to drifts in both the laser frequency and the interferometric path length [11]. The majority of previously reported I-PDV systems have used the sequential approach, with only the work by Seiler *et al.* [9] proposing a solution in the form of polarization multiplexing to capture a zero-flow reference image simultaneously with images of the flow. However, this approach suffers from crosstalk between the signal and reference channels, which distorts the phase measurements and requires a more complex setup using polarization-sensitive optics and a second camera.

Although frequency division multiplexing (FDM) has been applied in many fields, its application in full-field measurement instrumentation is limited, mainly due to restrictions in the available camera frame. Recently, we have demonstrated the technique in the area of full-field strain measurements [16], and a similar scheme has been described by Fischer *et al.* [17] to facilitate the measurement of multiple velocity components for molecular-filter-based PDV using optical frequency modulation.

Here, we propose and demonstrate an alternative FDM approach using amplitude modulation and its application to I-PDV. The technique not only allows the signal and reference channels to be acquired simultaneously on a single camera, but could be extended to facilitate full three-component, two-dimensional (planar) velocity measurements. This would require the multiplexing of four channels, three velocity channels, and a single reference channel, readily achievable using this approach. The aim of this work is to demonstrate the practicality of both aspects: the multiplexing of a signal and a reference channel, and the potential to measure multiple velocity components. The method is suitable for time-averaged flow measurements and has the added benefits of reduced camera noise and automatic background light suppression. Furthermore, it has the potential to be applied to molecular-filter-based PDV systems for the multiplexing of velocity channels.

## 2. FDM for I-PDV

FDM applied to imaging instrumentation [16] allows for the simultaneous capture of multiple interferometric fringe images using a single imaging sensor at full resolution, by applying an amplitude modulation that is unique to each channel to be multiplexed. A schematic of the concept is shown in Fig. 1. The system illustrated uses three illumination directions

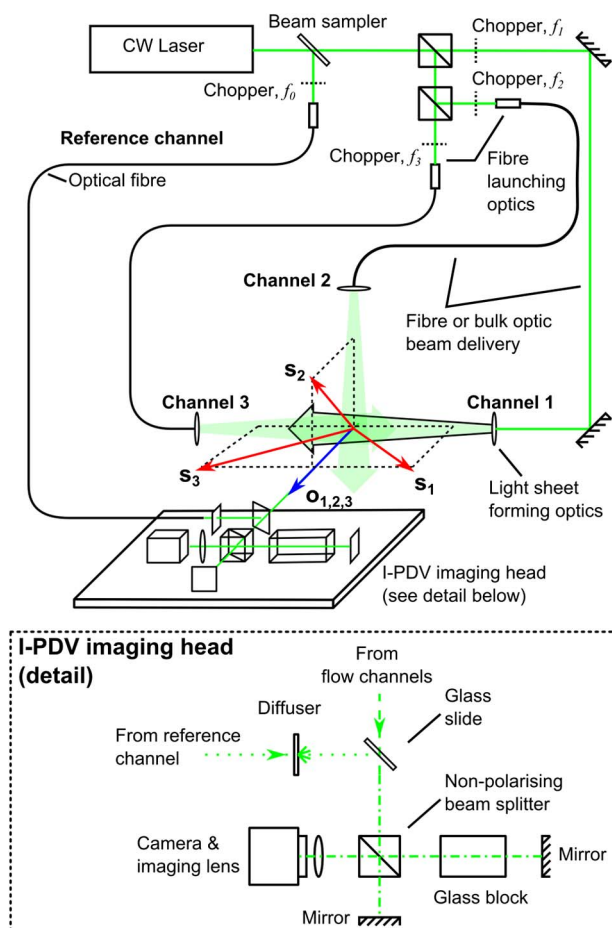


Fig. 1. Schematic showing the application of FDM to a general I-PDV system. Here, a three-velocity component system is shown using three signal channels illuminating the flow from different directions together with an unshifted reference channel. The channels are modulated here using beam choppers with the reference channel modulated at frequency  $f_0$  and the three measurement channels at frequencies  $f_1$ ,  $f_2$ , and  $f_3$ , respectively. Either bulk optics or fiber delivery can be employed to transport the beams to the light sheet forming optics.

and a single I-PDV imaging head to measure three different velocity components. The I-PDV imaging head shown uses a Michelson interferometer, as this is the most commonly reported configuration [10,13–15]. However the technique is equally applicable to single-component velocity measurements, and to the Mach–Zehnder interferometer (MZI) configuration previously reported [11,12] and used in the experimental section of this work.

A small fraction of the output from a high-power, single-frequency, and continuous wave (CW) laser is sampled to provide the reference illumination. The reference beam is amplitude modulated at frequency  $f_0$ , for example using a wheel chopper, before being guided to the interferometer input, typically using an optical fiber for ease of beam delivery. At the interferometer input, the reference beam is scattered by a diffuser to reduce speckle effects and enters the interferometer via reflection from the glass slide, ensuring uniform illumination across the field of view.

As this light comes directly from the laser, it will have zero Doppler frequency shift, and as such can be used to provide a reference phase measurement.

The remainder of the laser output is split into the required number of measurement channels, each of which is modulated at a distinct frequency. For a three-component PDV system, the light would be divided into three or more [18] channels and formed into light sheets to illuminate the flow. An example of this is illustrated in Fig. 1, where each channel illuminates the flow from a different direction, providing different sensitivity to the components of the flow velocity (illustrated in Fig. 1 by the vectors labeled  $s_1$ ,  $s_2$ , and  $s_3$ ). The three velocity component channels, 1–3, are shown modulated, using beam choppers at frequencies  $f_1$ ,  $f_2$ , and  $f_3$ , respectively, before being guided to light sheet forming optics.

The zero-shift reference light from the reference channel and the Doppler-shifted scattered light from each measurement channel are imaged through the interferometer and the combined fringe patterns recorded by the camera. The fringe patterns from each channel can then be demultiplexed by acquiring a time series of images over a number of modulation cycles, and using the process illustrated in Fig. 2.

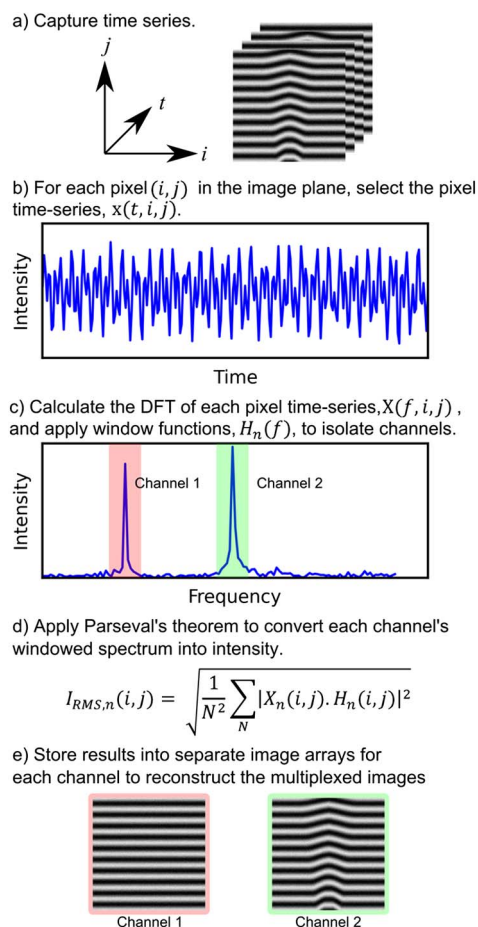


Fig. 2. Steps to demultiplex images from a FDM image time series. The example shown is for a single-velocity component system, consisting of two multiplexed channels.

The time series of a given pixel,  $x(t)$ , will vary in amplitude over time as a function of the number,  $n$ , of modulation frequencies present,

$$x(t) = \sum_n x_n(t) + C, \quad (4)$$

where  $x_n(t)$  is the time-varying signal from the  $n$ th channel and  $C$  is any nonmodulated background light intensity. To demultiplex the channels, the power spectrum is calculated via the discrete Fourier transform (DFT) on a pixel-by-pixel basis. The peaks corresponding to the modulation frequencies of the channels are separated using window functions, and their intensities are evaluated. The root mean squared (RMS) intensity of a channel's signal,  $I_{\text{RMS},n}$ , is calculated in the frequency domain using Parseval's theorem:

$$\begin{aligned} I_{\text{RMS},n} &= \sqrt{\frac{1}{N} \sum_N |x(t)|^2} = \sqrt{\frac{1}{N^2} \sum_N |X(f) \cdot H_n(f)|^2} \\ &= \sigma_n, \end{aligned} \quad (5)$$

where  $X(f)$  is the DFT spectrum of the signal  $x(t)$ ,  $N$  is the number of samples, and  $H_n(f)$  is the window function applied in the frequency domain to isolate the  $n$ th channel. As the background component of the signal is removed when windowing,  $I_{\text{RMS},n}$  is equivalent to the standard deviation of a channel's signal,  $\sigma_n$ . Hence, the peak-to-peak intensity  $I_{\text{pp},n}$  of the modulating signal can be found by dividing the extracted RMS intensity,  $I_{\text{RMS},n}$ , by the standard deviation of the normalized waveform,  $\sigma_{\text{cal}}$ , the theoretical or experimentally measured standard deviation of the modulation with a peak-to-peak amplitude of 1:

$$I_{\text{pp},n} = \frac{I_{\text{RMS},n}}{\sigma_{\text{cal}}}. \quad (6)$$

This step provides a useful quantity for the comparison of signal and noise levels between FDM and images recorded using continuous, nonmodulated illumination. However, in practice, this calculation is unnecessary as the RMS intensity is sufficient for measurements.

This process is repeated for each channel present, and the values placed into a separate image array for each channel. These images can then be considered to be equivalent to fringe patterns captured with only a single illumination channel present, and processed as in conventional I-PDV. The camera frame rate and the modulation frequencies used should be selected so as to not exceed the Nyquist condition and such that the peaks associated with individual channels can be resolved in the power spectrum. Consideration should also be given to the location of harmonics in the spectrum to limit between channels. This is discussed further in Section 5.

The technique demonstrated by Fischer *et al.* [17] used laser frequency modulation of multiple high power, tunable laser sources and a linear detector array that provided 25 measurement points capable of making measurements at 20 kHz. The technique proposed here uses amplitude modulation of a single laser source together with a 2D detector array, and thus is capable of measuring >100,000 pixels simultaneously at lower measurements rates of ~1 Hz. It should be noted, however, that the data rates demonstrated here and in [17] are a result of the technical realizations of the systems and not the measurement principles; indeed, there is no reason why the amplitude modulation scheme described here cannot be applied at higher frequencies and hence higher measurement rates. Also, in principle, the laser frequency modulation scheme described in [17] could be applied externally so that only a single laser would be necessary.

### 3. Experimental Arrangement

The experimental arrangement used is shown in Fig. 3. The laser source used was a high-power, external-cavity tapered diode laser (Sacher Lasertechnik Tiger) operating at 1.1 W CW output power at a wavelength of 780 nm. This was sampled using an antireflection-coated wedge, splitting off 1% of the beam power to provide the reference channel illumination. The reference beam was chopped using a mechanical chopper at frequency  $f_0 = 17.6$  Hz before being coupled into a single-mode optical fiber (Fibrecore SM750) and guided to the interferometer head. The output of the fiber illuminated a ground glass diffuser that rotated slowly (<5 Hz) to blur laser speckle, and entered the interferometer via reflection from a glass slide positioned in front of, and at 45° to, the imaging lens. The signal beam was chopped using a second mechanical chopper at frequency  $f_1 = 25.2$  Hz, and illuminated the flow after passing through a combination of cylindrical and spherical lenses to create a light sheet.

The FDM I-PDV technique was demonstrated by measuring a single velocity component of an axisymmetric air jet. The geometry is illustrated in Fig. 3, with the light sheet cutting across the jet flow at a 45° angle, and the interferometer collecting scattered light at an angle of 90° to the light sheet. This geometry gives a sensitivity vector that is aligned with the axis of the jet, but opposite to its flow, giving a Doppler frequency shift sensitivity of approximately 1.4 MHz per  $\text{ms}^{-1}$ . The jet used had a 20 mm diameter smooth contraction nozzle, and the air flow was seeded using a compact smoke generator (Concept Engineering Vicount), which generated "smoke" particles of liquid mineral oil with a diameter in the range of 0.2–0.3  $\mu\text{m}$ . By sliding the position of the jet nozzle forward and backward, the position of the measurement slice downstream of the nozzle exit could be varied, allowing the jet flow to be mapped. The jet was generated inside a chamber to contain the seeding particles.

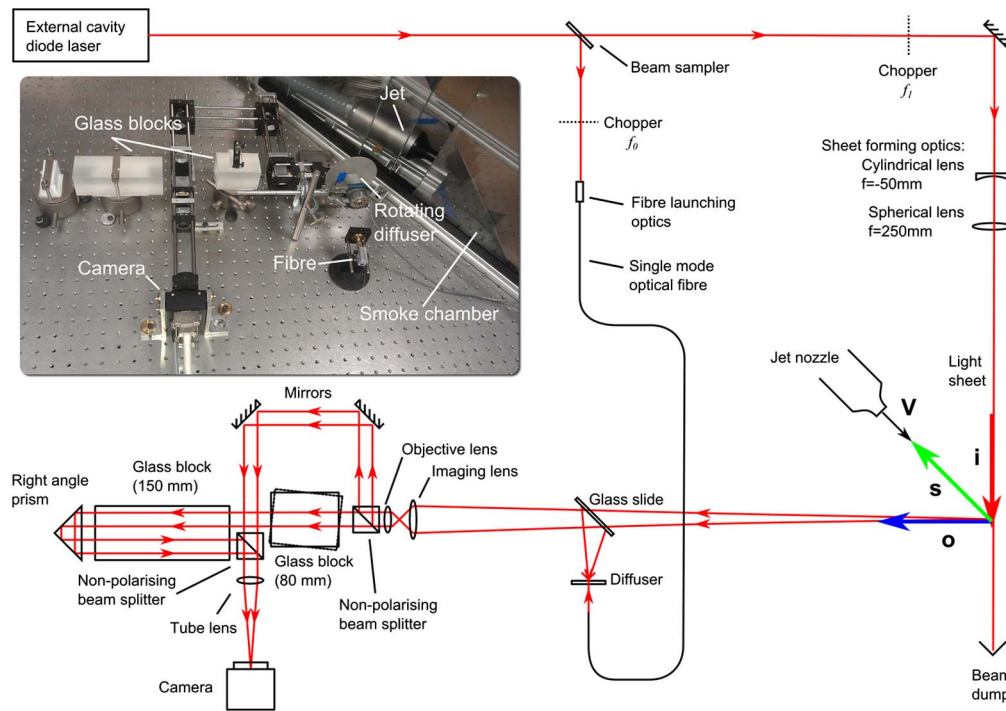


Fig. 3. Schematic showing the experimental FDM I-PDV system used. Inset is a photograph of the imaging MZI and the chamber containing the jet.

Scattered light was collected by an imaging MZI [11,12]. The MZI was constructed using an infinity-corrected optical system (Olympus PlanApo, 1.25 $\times$  objective with matched tube lens), which allows flexibility in the selection of the flow imaging optics without requiring modification of the interferometer itself. For example, we have previously demonstrated such imaging systems using a single imaging lens [12] or using imaging fiber bundles for multicomponent measurements [11]. The arrangement used here was modified from our previous work [11,12] to allow easier alignment, longer optical path difference, and the easier introduction of the linear carrier fringes required for the single interferogram, FFT-based phase evaluation method favored in I-PDV [11,13,15]. In addition to the 150 mm block used in the previous work, a second glass block (80 mm long) was placed in one arm of the interferometer in a single-pass arrangement. This glass block not only added extra optical path difference, but allowed the linear carrier fringes to be generated easily by tilting the 80 mm long block off-axis, with both the spatial frequency and direction of the fringes controlled by varying the tilt direction and magnitude. This was facilitated by the infinity-corrected optical system used, where light from a single object/image point traverses the region between the objective and tube lenses as a bundle of rays with a fixed angle with respect to the optical axis. A single pass through a tilted glass block adds a varying path length across the image, resulting in the required carrier fringe pattern. The total optical path difference was 360 mm, giving a FSR

of 833 MHz which, for the measurement geometry described previously, corresponds to a phase shift of approximately 0.01 radians per  $\text{ms}^{-1}$ . A Baumer HXC-13 CMOS camera (pixel size  $14 \times 14 \mu\text{m}$ ) was used to record the fringe patterns. The region of interest was  $328 \times 328$  pixels, which was selected to match the image size produced by the vignetting in the interferometer and the  $f = 25 \text{ mm}$ ,  $F = 1.6$  imaging lens used to image the flow. This gave a field of view of  $35 \times 35 \text{ mm}$ . The camera frame rate was set to 60 fps to achieve sufficient signal levels in the flow measurement channel, as the infinity-corrected interferometer had an inherent attenuation that increased with path length due to loss of higher-angle ray bundles.

The development and implementation of the signal processing was conducted in the open-source Python programming language [19], together with the NumPy and SciPy [20] modules. As typical data sets captured consist of large, three-dimensional arrays of signals with sizes approaching one gigabyte, the FDM demultiplexing algorithm was implemented in a bespoke shared library written in C using the FFTW3 library [21] in order to increase memory efficiency and speed. This was capable of demultiplexing the channels on the order of seconds. The demultiplexed fringe images were then processed using the Fourier domain processing described in our previous work [11] to calculate the signal and reference phases. The Doppler shift was then calculated from the phase shift and the FSR of the interferometer via Eq. (2), before an image dewarping algorithm was applied to remove perspective and

other distortions from the images [22]. The image dewarping was also used to determine the image scaling and sensitivity vectors for each pixel in the image [22]. Finally, the velocity component was calculated using the Doppler shift and sensitivity vectors via Eq. (1).

#### 4. Measurements on an Axisymmetric Air Jet

Image time series ( $N = 128$  frames) at each slice through the jet flow were acquired, with center positions at approximately 15, 24, 36, 47, 59, and 70 mm downstream from the nozzle exit plane. The recorded peak-to-peak intensity of the signal channel scattered from the flow was  $\sim 45$  counts in the center of the jet, dropping to  $\sim 10$  counts toward the edges of the jet. These were then processed, and the results are shown in Fig. 4. Due to the measurement geometry used, the jet nozzle impinged on the field of view on the left side of the slices at the 15 and 24 mm measurement positions. In Fig. 5, a vertical profile through the center of the each slice is shown as the dots (red). As the seeded air was extracted from the chamber, the air surrounding the jet was not stationary. Hence, a model of an axisymmetric compound jet [23] was implemented and fitted to each of

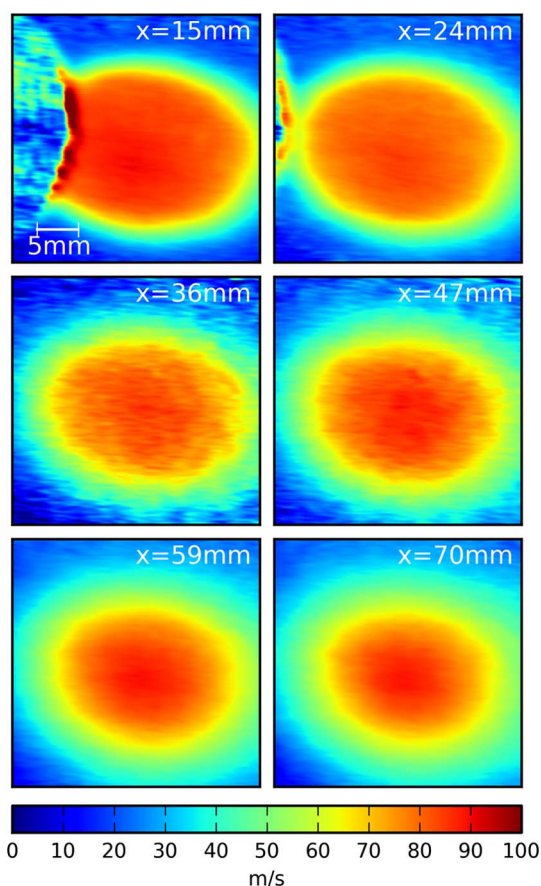


Fig. 4. Velocity measurements taken at  $45^\circ$  slices across the jet at different  $x$  positions of the center of the flow downstream from the nozzle. The field of view was  $35 \times 35$  mm. On the 15 and 24 mm images, the jet nozzle can be seen impinging in the field of view on the left side.

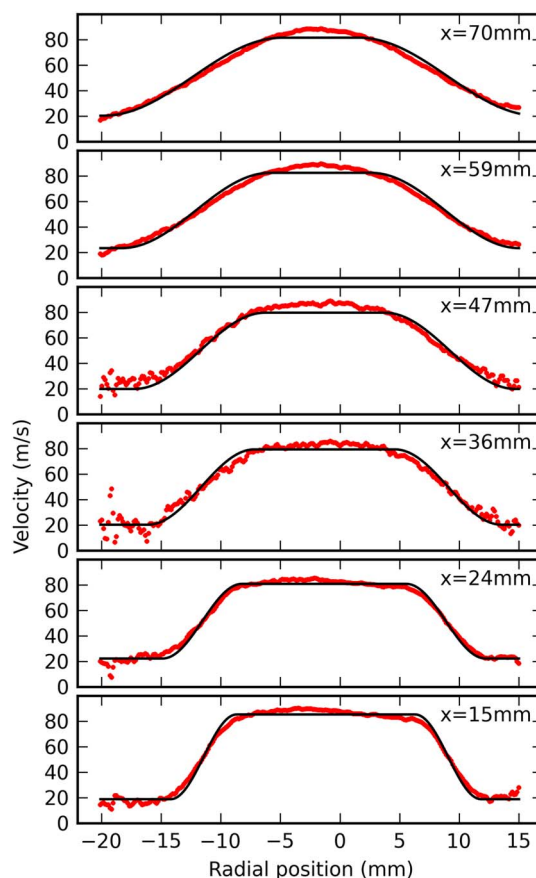


Fig. 5. Comparison of velocity profiles taken vertically through the center of the jet at different positions downstream from the nozzle (red points), and an empirical model (black lines) of an axisymmetric compound air jet [23].

the measured profiles. These are shown as the solid lines (black) in Fig. 5. For the fitted profiles, a jet exit velocity of around  $79\text{--}85\text{ ms}^{-1}$  was found along with a surrounding flow of  $19\text{--}23\text{ ms}^{-1}$ . The results showed that the expected top-hat velocity structure was present near the nozzle, becoming smoother as the jet developed, and this was in good agreement with the model. This experiment demonstrated that the signal and reference fringe patterns can be successfully multiplexed using the FDM technique.

#### A. Influence of Interferometric Phase Drifts During the Acquisition Period

The slices at  $x = 36$  mm and  $x = 47$  mm in Fig. 4 show increased noise in comparison with the other measurements, and this can also be seen in the profiles plotted in Fig. 5. This appears to be due to a reduction in the demultiplexed fringe visibility at these locations. Figure 6 shows a closeup of the demultiplexed reference channel fringes for the  $x = 15$  mm and  $x = 47$  mm slices. Here it can be seen that the fringe visibility has dropped significantly, from a range of  $\sim 32$  counts for the measurement at 15 mm to  $\sim 8$  counts for the measurement at 47 mm. In addition, the position of the fringes can be observed to have shifted, suggesting a drift

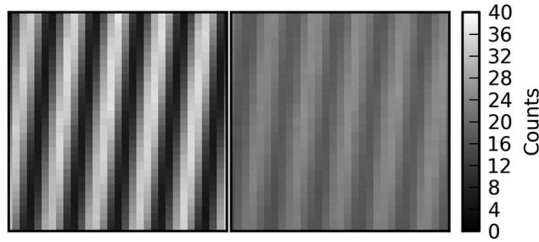


Fig. 6. Enlarged regions of the demultiplexed reference fringes. Left image shows fringes 15 mm downstream with a low drift. Right image shows fringes at 47 mm demultiplexed with a higher drift.

between the two measurements. The measurement at 47 mm was acquired approximately halfway through an extended testing session lasting approximately 30 min, with the laser, air jet, smoke generator, and extractor fan running continuously throughout. As such, the most likely cause is that the laboratory environment changed, resulting in an interferometric phase drift during the acquisition period of the image time series. Measurements made later during the same testing session show better fringe visibility and noise levels, suggesting that the phase drift had stabilized by the time of these measurements.

Considering the effect of such a drift in FDM, it can be shown that if the fringe phase drifts by  $2\pi$  during the acquisition period, then the visibility of the demultiplexed fringes will be completely reduced to zero. Smaller phase drifts will result in a less dramatic reduction in visibility. By using a simple model of a one-dimensional fringe pattern and calculating the fringe positions at each frame of an FDM time series, the expected fringe visibility for a given drift can be calculated; the results are shown in Fig. 7. From this, it can be seen that, as long as the phase drift remains small during the acquisition period, loss of fringe visibility should not be an issue. To put the level of acceptable drift into context for the measurements presented here, a drift of  $2\pi$  would require the laser frequency to drift by 416.5 MHz/s, which is much greater than the expected performance of the temperature-stabilized diode laser system of  $\sim 0.75$  MHz/s [24]. It is also worth noting the interferometer was not actively stabilized, so stabilization systems such as those employed by Lu *et al.* [12] could be employed to prevent or reduce drift during data acquisition.

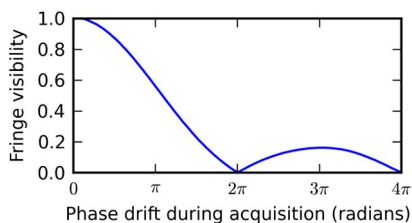


Fig. 7. Calculated FDM fringe visibility for varying levels of phase drift during data acquisition.

## B. Camera Noise

It was anticipated that the FDM technique may have some favorable characteristics with regard to the level of camera noise in the demultiplexed images, due to the windowing/bandpass filtering applied as a consequence of the demultiplexing process. To examine the camera's noise characteristics when using the FDM technique, a lens cap was placed over the camera sensor, and an image time series was captured under the measurement conditions used above (60 fps, 16661  $\mu$ s exposure time,  $N = 128$  frames). From this, the two measurement channels were demultiplexed to give a measurement of the camera noise present in each channel. This was repeated to give 100 measurements from which the background level and standard deviation of a typical camera pixel, shown in Tables 1(a) and 1(b), can be found. As the camera used was a CMOS sensor, each pixel has individual noise characteristics; hence, the typical values presented here are the mean values for all pixels. For comparison, the background and standard deviations for single exposure measurements and for the average of  $N = 128$  frames are shown in Tables 1(e) and 1(f), respectively.

It can be seen that the FDM process suppresses the pixel background level and that the remaining noise is reduced significantly when compared to a single-frame measurement, and reduced slightly compared to simply averaging 128 frames. This is an expected consequence of the application of the windowing/bandpass filtering in the demultiplexing process. However, it is important to note that the signal amplitude measured via FDM is the RMS amplitude, not the peak amplitude measured when averaging a nonmodulating signal. Hence, when the FDM noise levels are scaled via Eq. (6), the SNR for the FDM measurements, shown in Tables 1(c) and 1(d), will be slightly worse than simply averaging the same number of frames.

## C. Channel Crosstalk

A further important potential source of error is the crosstalk between measurement channels. In the

Table 1. Noise Characteristics of a Typical Camera Pixel Using FDM Demultiplexing at (a)  $f = 17.6$  Hz and (b)  $f = 25.2$  Hz, with a 1.5 Hz Window<sup>a</sup>

Method	Mean Background Level (Counts)	Standard Deviation (Counts)
(a) FDM channel 1, $I_{\text{RMS}}$	0.11	0.027
(b) FDM channel 2, $I_{\text{RMS}}$	0.09	0.027
(c) FDM channel 1, $I_{\text{PP}}$	0.25	0.064
(d) FDM channel 2, $I_{\text{PP}}$	0.21	0.063
(e) Single frame	3.32	0.440
(f) Frame averaging (128 frames)	3.32	0.054

<sup>a</sup>Rows (c) and (d) show the same values scaled to the peak amplitude of the modulation for comparison purposes with (e) single frame measurements and (f) the average of 128 frames, respectively.

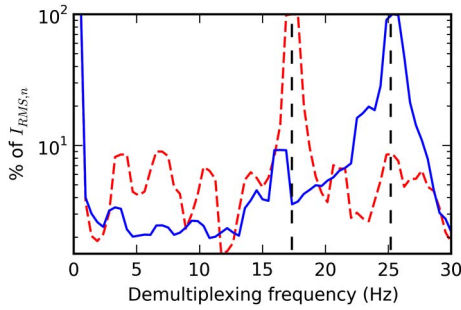


Fig. 8. Signal leakage (crosstalk) as a percentage of the channel's RMS intensity,  $I_{RMS,n}$ , into other demultiplexing frequencies. Crosstalk from the reference channel (17.6 Hz peak) is shown by the red/dashed line and crosstalk from the signal channel (25.2 Hz) is shown by the blue/solid line. The center frequencies of the signal and reference channels are shown by the vertical dashed lines.

work by Seiler *et al.* [9], in which polarization division multiplexing (PDM) was used to separate the signal and reference fringe patterns, incomplete separation of the two images is reported but the level of this crosstalk is not quantified. However, in similar full-field imaging instrumentation using PDM, crosstalk of up to 20% has been reported [25]. To measure the level of crosstalk using the FDM technique, an image time series was recorded for each of the two channels with only one channel present in each. From each of these time series, an image was demultiplexed at the modulation frequency of the illuminating channel, and was used as the measure of the signal for that channel. The level of crosstalk from the channel could then be evaluated by demultiplexing images at other frequencies. The results are shown in Fig. 8, where the crosstalk resulting from channel 1 (17.6 Hz) and channel 2 (25.2 Hz) are shown for all demultiplexing frequencies possible. The FDM crosstalk from a channel is typically below 10%, with minima of around 1.5%, which compares favorably with reported levels of crosstalk when using PDM. In this work, the crosstalk was 3.6% and 8.1% for channels 1 and 2, respectively, although this could in principle be improved by adjusting the channel frequencies to correspond to a minimum in the crosstalk spectrum.

## 5. Extension to Multiple Velocity Components

In Section 2, the multiplexing of additional velocity components using FDM was proposed. To achieve this, it would be necessary to use one FDM signal channel per velocity component, plus one more for the reference channel, which is common to all signal channels. For example, for a three-velocity component system, four FDM channels would be required. The feasibility of applying FDM in these circumstances was then investigated using the experimental system described previously.

### A. Camera Dynamic Range

The first issue to consider when expanding the technique to four or more channels is the dynamic range

of the camera, as the amplitude of an individual channel is limited to  $1/n_{\text{channels}}$  of the available range. For example, in a system using an 8 bit camera with four channels, each channel can have a maximum peak-to-peak amplitude of 63 counts. In order to determine if this is sufficient, it is necessary to consider the noise present in FDM measurements. Expressions for the standard deviation of the noise in FDM measurements can be found via the propagation of errors through Eqs. (5) and (6) and using [26]

$$\sigma_{\text{RMS}} = \frac{\sigma_x}{\sqrt{2N}}, \quad (7)$$

$$\sigma_{\text{pp}} = \frac{\sigma_x}{\sigma_{\text{cal}} \sqrt{2N}}, \quad (8)$$

Here,  $\sigma_x$ ,  $\sigma_{\text{RMS}}$ , and  $\sigma_{\text{pp}}$  are the standard deviations in a single measurement, the computed RMS intensity, and the peak-to-peak intensity, respectively.  $N$  is the number of frames in the time series and  $\sigma_{\text{cal}}$  is the standard deviation of the normalized waveform used to scale the signals to peak-to-peak intensities. For comparison, the standard deviation of the noise level when frame averaging,  $\sigma_{\text{AVG}}$ , can also be expressed as

$$\sigma_{\text{AVG}} = \frac{\sigma_x}{\sqrt{N}}. \quad (9)$$

Both the theoretical noise levels and experimental measurements, scaled to the peak-to-peak intensities, are shown in Fig. 9 for various values of  $N$ . While there is good agreement between the theory and the experimentally measured points, the results for frame averaging diverge for larger values of  $N$ , possibly due to the presence of drifts in the pixel amplifier gains becoming apparent over longer time-scales. It can be seen from Eq. (7) that the noise level in the FDM measurements is independent of the width of the window function used in the demultiplexing. However, in practice, the window width will

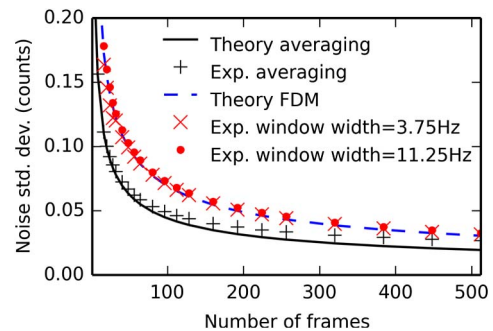


Fig. 9. Noise standard deviation versus number of frames in the time series,  $N$ . The solid lines show the theoretical noise propagation for frame averaging (solid/black) and FDM scaled to the peak-to-peak intensity (dashed/blue), and experimental results are shown using two FDM window widths, 3.75 Hz (red crosses) and 11.25 Hz (red dots), and frame averaging (black crosses).

influence the signal-to-noise ratio (SNR) of a measurement if the noise power spectrum contains peaks at distinct frequencies that lie within the window function used. Similarly, if the channel's power is spread beyond the window used, via peak broadening or higher harmonics, then the recovered signal intensity will be lower and the SNR will be reduced.

In comparison with the frame averaging method, the SNR level in an FDM measurement will be slightly lower when using the same number of frames. However, it should be remembered that, in contrast with FDM, only sequential recording of channels is possible with this averaging approach, and that if  $m$  channels are to be measured within the same acquisition period, only the average of  $N/m$  frames can be used. Using Eqs. (8) and (9), it can be seen that the number of channels required for the FDM noise to be equal to or less than that of using sequential recording and that for frame averaging the number of channels can be found from

$$\frac{\sigma_x}{\sigma_{\text{cal}} \sqrt{2N}} \leq \frac{\sigma_x}{\sqrt{\frac{N}{m}}}, \quad (10)$$

$$m \geq \frac{1}{2\sigma_{\text{cal}}^2}. \quad (11)$$

For square wave modulations with only the fundamental peak included in the window function,  $\sigma_{\text{cal}} \sim 0.45$  and, in these circumstances, the noise performance of FDM is favorable when three or more channels are multiplexed. This was also observed experimentally, with Table 2 showing the noise levels (scaled to peak-to-peak amplitudes) for  $(n/m) = 128$ , 64, 42, and 32 frames corresponding to measurements of one, two, three, and four channels recorded sequentially in the same acquisition time as the FDM measurement.

Frankowski *et al.* [27], report that, for a digitization of 6 bits ( $I_0 = 63$  counts), a standard deviation in the phase measurement of better than 0.006 radians can be achieved when using the FFT-based phase evaluation method discussed in Section 4, which corresponds to a velocity uncertainty of  $\sim 0.6 \text{ ms}^{-1}$  for the MZI system described in Section 3. The

**Table 2. Experimental Comparison of the Noise Standard Deviation for a Typical Camera Pixel When Using FDM Demultiplexing (shown in bold) and Frame Averaging Measurements of 1, 2, 3 and 4 Channels Recorded Sequentially in the Same Acquisition Time**

Method	Standard Deviation (Counts)
Frame averaging, 1 channel, $I_{\text{Avg}, N=128}$	0.044
Frame averaging, 2 channels, $I_{\text{Avg}, N=64}$	0.059
<b>FDM, <math>I_{\text{pp}}</math></b>	<b>0.063</b>
Frame averaging, 3 channels, $I_{\text{Avg}, N=42}$	0.071
Frame averaging, 4 channels, $I_{\text{Avg}, N=32}$	0.081

modulation's peak-to-peak intensity  $I_{\text{pp}, n}$  required to give the same SNR, and hence velocity uncertainty, as a single exposure measurement with an intensity,  $I_0$ , can be determined by equating the SNRs in each case:

$$\frac{I_0}{\sigma_x} = \frac{I_{\text{pp}}}{\sigma_{\text{pp}}}, \quad (12)$$

$$I_{\text{pp}} = \frac{I_0}{(\sigma_{\text{cal}} \sqrt{2N})}. \quad (13)$$

Applying Eq. (13) with  $I_0 = 63$  counts,  $N = 128$ , and  $\sigma_{\text{cal}} \sim 0.45$  gives an equivalent SNR when  $I_{\text{pp}} \sim 9$  counts. To demonstrate this experimentally, examples of a single row through a demultiplexed fringe pattern are shown in Fig. 10 for  $I_{\text{pp}}$  amplitudes of 64, 32, 16, and 8 counts. It can be seen that the fringe pattern is still clearly visible at 8 counts. If the full dynamic range available was used,  $I_{\text{pp}} = 63$  counts, then the FDM measurement would have a SNR equal to a single exposure measurement with  $I_0 = 450$  counts. Therefore, it can be concluded that there is sufficient dynamic range available for the multiplexing of the four channels required for three-component velocity measurements, even in the presence of a strong background signal.

#### B. Crosstalk and Bandwidth Considerations

The second consideration is whether there is sufficient bandwidth to multiplex the required number

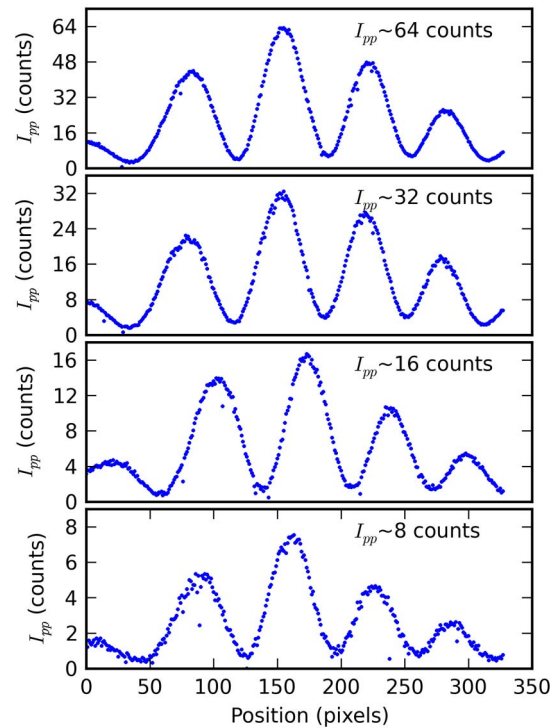


**Fig. 10.** Plots of a single row of a fringe pattern recorded using FDM for various peak amplitudes,  $I_{\text{pp}}$ .

of channels and that the resulting crosstalk is not excessive. This was investigated by considering the power spectra under different combinations of channel modulation frequencies and ensuring that the channels were not colocated with harmonics from the other channels. To demonstrate this experimentally, and to evaluate the expected level of crosstalk achievable, image time series with only a single channel present in each were recorded for four FDM channels, at frequencies 5, 12, 20, and 29 Hz, with equal peak-to-peak modulation amplitudes. The resulting channel power spectra were calculated, and from these, the total crosstalk into one channel with a given demultiplexing frequency from the other three channels was estimated by summing the power spectra of the other three channels. The results are shown in Fig. 11, for two values of  $N$ :  $N = 128$  (red/dashed lines) and  $N = 256$  (blue/solid lines). Here, the total crosstalk is scaled to a percentage of the channel's RMS signal. Also shown as the shaded areas are the power spectra of the channel calculated at  $N = 128$  (red/hatched shading) and  $N = 256$  (blue/solid shading), allowing the location of the channel relative to the crosstalk spectrum to be seen. The total crosstalk for each channel is shown in Table 3. For  $N = 128$  frames, the total crosstalk for each channel is  $\sim 20\%$  or less, which is comparable with the level of crosstalk achieved using PDM for two channels [25]. If  $N$  is increased, the power

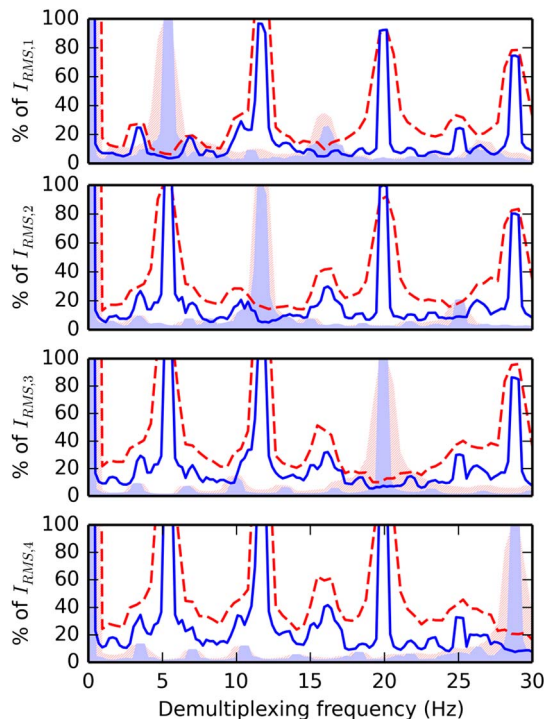


Fig. 11. Experimental crosstalk spectra between four FDM channels. The lines show the total crosstalk into a channel from the other three channels as a percentage of the channel's RMS intensity,  $I_{\text{RMS},n}$ , at  $N = 128$  frames (red/dashed lines) and  $N = 256$  frames (blue/solid lines). Also shown, as the shaded areas, are the power spectrums of the channel itself calculated at  $N = 128$  (red/hatched shading) and  $N = 256$  (blue/solid shading).

Table 3. Total Crosstalk as a Percentage of the Channel's RMS Intensity,  $I_{\text{RMS},n}$ , for Four Channels of Equal Peak Intensity

$N$ (frames)	Channel Frequency			
	5 Hz	12 Hz	20 Hz	29 Hz
128	6.8%	16.0%	10.1%	20.5%
256	4.3%	5.2%	6.4%	8.2%

spectrum peaks become sharper and more localized, reducing the spread of frequencies and hence reducing crosstalk. It can be seen from Fig. 11 and the values in Table 3 that increasing  $N$  to 256 frames resulted in significantly lower crosstalk, with all channels now below 10% and comparable with the crosstalk levels measured in the two channel results presented above.

In practice, the influence of crosstalk on the measurement of interferometric phase is complicated and will depend upon a number of factors, including the relative channel intensities, modulation waveform, the Doppler shift, and the phase evaluation method used. The amplitude of a channel will directly scale the level of crosstalk to other channels, and similarly, the Doppler shift present will change the intensity of a given pixel due to the resulting interferometric phase shift. This can result in the shape of fringes becoming distorted and introduce errors in the phase measurements. Hence, it is conceivable that the magnitude of these errors will differ with the choice of evaluation method, e.g., spatial carrier fringe/Fourier domain processing or phase stepping. This requires further investigation to determine the likely effects. It may be necessary to increase  $N$  to minimize crosstalk between channels when multiplexing additional channels.

Another important point to note is that, unlike PDM, where the crosstalk is mainly due to depolarization of the scattered light and is thus unknown and potentially variable, crosstalk in FDM is due to the power spectra of the modulations used. As this should remain constant and is measurable, it may be possible to correct for the effects of crosstalk in post-processing. By considering the demultiplexed intensity as combinations of contributions from each channel, it can be seen that this results in the matrix equation

$$\begin{bmatrix} I'_{\text{RMS},1} \\ I'_{\text{RMS},2} \\ I'_{\text{RMS},3} \\ I'_{\text{RMS},4} \end{bmatrix} = \begin{bmatrix} 1 & C_{21} & C_{31} & C_{41} \\ C_{12} & 1 & C_{32} & C_{42} \\ C_{13} & C_{23} & 1 & C_{43} \\ C_{14} & C_{24} & C_{34} & 1 \end{bmatrix} \begin{bmatrix} I_{\text{RMS},1} \\ I_{\text{RMS},2} \\ I_{\text{RMS},3} \\ I_{\text{RMS},4} \end{bmatrix}. \quad (14)$$

Here,  $I'_{\text{RMS},n}$  is the demultiplexed RMS intensity of channel  $n$ , including crosstalk from other channels;  $I_{\text{RMS},n}$  is the desired RMS intensity of the channel excluding crosstalk; and  $C_{mn}$  is the crosstalk from channel  $m$  to channel  $n$ , which can be found by calibration.

This can be solved to recover the channel intensities,  $I_{\text{RMS},n}$ , and minimize the effects of crosstalk.

## 6. Conclusions

A new method of multiplexing the signal and reference fringe patterns required for I-PDV using FDM has been developed and demonstrated with single-component velocity measurements on an axisymmetric air jet. The results show good agreement with an empirical model of the jet. Interferometric phase drifts were identified as a possible cause of increased noise levels in measurements, although this could easily be minimized in a refined system via phase stabilization. The FDM technique was also shown to suppress background light levels and reduce the effective camera noise as a consequence of the windowing/filtering process used to demultiplex multiple channels. The velocity uncertainty achievable using the current system can be estimated to be better than  $0.6 \text{ ms}^{-1}$  for the interferometer and phase processing scheme used. Finally the crosstalk between the signal and reference channels was measured to be  $<10\%$ , which compares favorably with reported levels of crosstalk using polarization multiplexing of  $\sim 20\%$ .

Issues that may affect the expansion of the scheme to allow the multiplexing of additional velocity components were addressed. Expressions for the camera noise present in an FDM measurement were presented, with the noise level in an FDM measurement being marginally worse than frame averaging the same number of frames ( $\sigma_{\text{FDM,pp}} = 0.063$  counts versus  $\sigma_{\text{AVG}} = 0.044$  counts). However, as FDM allows multiple channels to be multiplexed using the same  $N$  frames, the noise performance of FDM is favorable compared to frame averaging and sequential recording in the same acquisition period, when three or more channels are multiplexed (for example, for  $m = 4$  channels, the noise levels are  $\sigma_{\text{FDM,pp}} = 0.063$  counts versus  $\sigma_{\text{AVG}} = 0.081$  counts). The dynamic range limitation of the camera was investigated, and the 63 counts available per channel when using an 8 bit camera and multiplexing four channels was determined to be more than sufficient to allow velocity uncertainties of  $<0.6 \text{ ms}^{-1}$ . Finally it was shown that, by careful consideration of the channel frequencies, it is possible to multiplex four channels with crosstalk levels of 10% or less using  $N = 256$  frames. Additionally, as the crosstalk is dependent upon the modulation used, it should be possible to compensate for it via calibration and post-processing.

The authors acknowledge the support of the Engineering and Physical Sciences Research Council (EPSRC) UK via grant EP/G033900/1 and a studentship for IAB. (For enquiries relating to access to the research data or other materials referred to in this article, please contact Cranfield University Library and Information Services—[library@cranfield.ac.uk](mailto:library@cranfield.ac.uk)).

## References

1. T. O. H. Charrett, S. W. James, and R. P. Tatam, "Optical fibre laser velocimetry: a review," *Meas. Sci. Technol.* **23**, 032001 (2012).
2. G. S. Elliott and T. Beutner, "Molecular filter based planar Doppler velocimetry," *Prog. Aerosp. Sci.* **35**, 799–845 (1999).
3. M. Samimy and M. P. Wernet, "Review of planar multiple-component velocimetry in high-speed flows," *AIAA J.* **38**, 553–574 (2000).
4. J. F. Meyers and H. Komine, "Doppler global velocimetry: a new way to look at velocity," in *Proceedings of the ASME Fourth International Conference on Laser Anemometry, Advances and Applications*, Cleveland, Ohio, August 5–9, 1991, Vol. 1, pp. 289–296.
5. M. S. Reinath, "Doppler global velocimeter development," *Meas. Sci. Technol.* **12**, 432–441 (2001).
6. V. Chan, A. Heyes, D. Robinson, and J. Turner, "Iodine absorption filters for Doppler global velocimetry," *Meas. Sci. Technol.* **6**, 784–794 (1995).
7. J. F. Meyers and J. W. Lee, "Investigation of measurement errors in Doppler global velocimetry," in *SAE World Aviation Congress and Exposition* San Francisco, California, October, 1999.
8. F. Seiler, A. George, F. Leopold, J. Srulijes, and G. Smeets, "Flow velocities visualization using Doppler picture interference velocimetry," in *ICIASF 99. 18th International Congress on Instrumentation in Aerospace Simulation Facilities* (IEEE, 1999), pp. 11/1–11/8.
9. F. Seiler, A. George, J. Srulijes, and M. Havermann, "Progress in Doppler picture velocimetry (DPV) technique," in *Proceedings of the 12th International Symposium on Flow Visualization*, Göttingen, Germany (2006), pp. 1–10.
10. A. Pichler, A. George, F. Seiler, J. Srulijes, and M. Havermann, "Doppler picture velocimetry (DPV) applied to hypersonics," in *Shock Waves SE—80*, K. Hannemann and F. Seiler, eds. (Springer, 2009), pp. 503–508.
11. Z. Lu, T. O. H. Charrett, and R. P. Tatam, "Three-component planar velocity measurements using Mach-Zehnder interferometric filter-based planar Doppler velocimetry (MZI-PDV)," *Meas. Sci. Technol.* **20**, 034019 (2009).
12. Z. Lu, T. O. H. Charrett, H. D. Ford, and R. P. Tatam, "Mach-Zehnder interferometric filter based planar Doppler velocimetry (MZI-PDV)," *J. Opt. A* **9**, 1002–1013 (2007).
13. A. Landolt and T. Roesgen, "Global Doppler frequency shift detection with near-resonant interferometry," *Exp. Fluids* **47**, 733–743 (2009).
14. A. Landolt and T. Roesgen, "Anomalous dispersion in atomic line filters applied for spatial frequency detection," *Appl. Opt.* **48**, 5948–5955 (2009).
15. F. Seiler, A. Pichler, R. Pfaff, and A. George, "Improved Doppler picture velocimetry and new automated processing," in *14th International Symposium on Application of Laser Techniques to Fluids*, Lisbon, Portugal (2008), pp. 7–10.
16. I. A. Bledowski, T. O. H. Charrett, D. Francis, S. W. James, and R. P. Tatam, "Frequency-division multiplexing for multi-component shearography," *Appl. Opt.* **52**, 350–358 (2013).
17. A. Fischer, L. Büttner, and J. Czarske, "Simultaneous measurements of multiple flow velocity components using frequency modulated lasers and a single molecular absorption cell," *Opt. Commun.* **284**, 3060–3064 (2011).
18. T. O. H. Charrett, D. S. Nobes, and R. P. Tatam, "Investigation into the selection of viewing configurations for three-component planar Doppler velocimetry measurements," *Appl. Opt.* **46**, 4102–4116 (2007).
19. Python Software Foundation, "Python Programming Language—Official Website," <http://www.python.org/>.
20. "SciPy—Scientific Tools for Python," <http://www.scipy.org/>.
21. M. Frigo and S. G. Johnson, "FFTW—Fastest Fourier transform in the west," <http://www.fftw.org/>.
22. D. S. Nobes, B. Wieneke, and R. P. Tatam, "Determination of view vectors from image warping mapping functions," *Opt. Eng.* **43**, 407–414 (2004).
23. N. Rajaratnam, *Turbulent Jets* (Elsevier, 1976), Vol. 5, Chap. 4, pp. 63–86.

24. Sacher Lasertechnik Group, Pilot PC Laser Driver User Manual (2008).
25. R. M. Groves, S. W. James, and R. P. Tatam, "Polarization-multiplexed and phase-stepped fibre optic shearography using laser wavelength modulation," *Meas. Sci. Technol.* **11**, 1389–1395 (2000).
26. G. Betta, C. Liguori, and A. Pietrosanto, "Propagation of uncertainty in a discrete Fourier transform algorithm," *Measurement* **27**, 231–239 (2000).
27. G. Frankowski, I. Stobbe, W. Tischer, and F. Schillke, "Investigation of surface shapes using a carrier frequency based analysing system," *Proc. SPIE* **1121**, 89–100 (1990).

# Frequency division multiplexing for interferometric planar Doppler velocimetry

Charrett, Thomas O. H.

2014-05-30

Attribution-NonCommercial-NoDerivatives 3.0 International

---

Charrett TOH, Bledowski IA, James SW, Tatam RP. (2014) Frequency division multiplexing for interferometric planar Doppler velocimetry. *Applied Optics*, Volume 53, Issue 20, July 2014, pp. 4363-4374

<http://dx.doi.org/10.1364/AO.53.004363>

*Downloaded from CERES Research Repository, Cranfield University*